STRUCTURAL OPTIMIZATION OF MICROJET ARRAY COOLING SYSTEM

Tomasz Muszynski[1], Dariusz Mikielewicz[1]

1: Gdansk University of Technology, Faculty of Mechanical Engineering, Department of Energy and Industrial Apparatus

Narutowicza 11/12, 80-233 Gdansk, Poland

E-mail: Tomasz.Muszynski@pg.gda.pl, Dariusz.Mikielewicz@pg.gda.pl,

ABSTRACT

The single phase heat transfer from an upward facing, horizontal copper surface to arrays of impinging water jets was experimentally investigated. Experimental configuration allows for a free-surface unconfined jets flow. Square nozzles 50x100μm arranged in four different geometries were used. Additionally, for the set of two jets array geometry was varied by adjusting the nozzle to nozzle distance. The area averaged heat transfer coefficient was found to be a strong function of working fluid mass flux and array geometrical aspect ratio. The proposed correlation agreed with the experimental data within 30% error bounds Obtained database of experimental data with analytical correlation allows the rational design of microjet modules for various industrial applications.

Introduction

Novel, advanced, high power technologies require a large amount of heat to be dissipated from the finite surface area. Thus, a new generation of thermal management systems is essential to further development of various technologies [1]. Research regarding dissipation of high heat fluxes is focused amongst other on using spray cooling [2,3], microchannels [4], microjets [5,6] and combined techniques [7,8]. Liquid jet impingement is one of the most effective means of achieving very high convection coefficients, especially when the coolant undergoes phase change [6]. Choice of jet configuration is based on several practical considerations including operating environment, coolant compatibility, and, of course, heat

dissipation and surface temperature. The jet typically impinges the heat–dissipating surface through a circular or a rectangular orifice [9]. The convection coefficient is highest in the impact zone directly below the jet orifice and diminishes while increasing distance from the impact zone. The average heat transfer coefficient for a large surface can be increased substantially and the surface temperature rendered more uniform by using multiple jets [10].

While jets can demand higher coolant flow rates than competing high-performance cooling schemes [2], they do offer significant advantages. For example, compared to micro-channel flow, they facilitate the removal of very high heat fluxes with relatively modest pressure drops [7]. This advantage is even more pronounced when compared to the two-phase flows in channels [11]. Furthermore, microjets are highly adaptable to cooling multiple devices in a compact package, ensure temperature uniformity when using multiple confined jets, and are applicable to both terrestrial and microgravity environments, as well as can endure the severe body forces induced by military aircraft maneuvers. Many of recent papers [12] are devoted to investigating microjet cooling, which may answer to industry demands.

The research team led by Michna [13] obtained pressure drop and area-averaged heat transfer data for a single confined, submerged 67-μm diameter jet of water which impinged on an 80-μm square heater. Reynolds numbers in the range $40 < Re_D < 1900$ were investigated. Area-averaged heat fluxes up to 400 W/m^2 were obtained with inlet fluid to surface temperature differences of about 50K, but the Nusselt numbers measured were much lower than predicted by macroscale jet correlations. The dependency of the Nusselt number on the Reynolds number was also weaker than those observed for macro scale jets.

Whelan and Robinson [14] have focused on the influence of the inlet and outlet geometries on the thermal-hydraulics of jet impingement heat transfer. Experiments were conducted with a square array of 45 jets of fixed 1.0mm diameter and fixed inter-jet spacing of 5 mm, six different nozzle geometries were investigated. All nozzles were tested for a Reynolds number range of approximately $800 < Re < 10\,000$. Authors found that the confined-submerged tests yield greater heat transfer coefficients compared with their free jet counterparts.

Detailed heat transfer distributions under arrays of jets impinging on a target plate with were investigated by Gillespie et al. [15]. They found that the cross flow and the exit flow direction significantly affect the heat transfer distributions on a target surface.

The microjet impingement was used to enhance heat transfer rate in a liquid-to-liquid heat exchanger by Muszynski and Andrzejczyk [16]. Microjets were formed by 600μm orifices, with orifice area to the heat transfer surface ratio of 0.3%. During experiments, the heat exchanger was capable of obtaining overall heat transfer coefficient up to 10 000 W/m^2K. For cylindrical setup [17] with similar size of microjets and area ratio of 2%, the heat transfer coefficient reaches over 12 000W/m^2K.

Recently Tran et.al [18] presented CFD optimization and experimental results of a microjet enhanced microchannel heat exchanger. The optimized heat exchanger was capable of transferring up to 500 W of heat per base area of 1 cm^2. Karwa et. al [19] presented CFD simulations and experimental investigations of a 3D printed prototype microjet heat sink with microjet technology. The research was performed with the aim to obtain a lowest thermal resistance, which for proposed heat sink was 0.025 K/W at the pressure drop of 25 kPa.

The main objective of this paper was to investigate the physical phenomena occurring on solid surfaces upon impingement of the water microjet arrays. The article presents a systematic experimental study of arrays geometrical dimensions on heat transfer at the impinged surface.

Presented tests were conducted under steady state conditions for surface cooling by multiple e microjets with varying geometrical dimensions. Obtained database of experimental data with analytical solutions and numerical computer simulation allows the rational design and optimization of microjet thermal management systems for various industrial applications. A simple theoretical model of the considered phenomenon has also been proposed. The study was conducted in a laboratory built at the Department of Energy and Industrial Apparatus of Gdansk University of Technology.

Experimental setup

The present study shows the results of steady state heat transfer experiments, conducted for single phase cooling in order to obtain wall temperature and heat fluxes. Fig. 1 shows the schematic diagram of the test section. It consisted of the probe, the fluid supplying system, the measuring devices and DC power supply. Working fluid was fed to the nozzle array from a supply tank, which also serves as the pressure accumulator. The water pressure in the test section was controlled by adjusting the air pressure in pressure accumulator. The desired fluid flow rate was obtained by sustaining the constant pressure of the fluid with a proper use of flow control valves. In order to reduce pressure drop necessary to create a steady laminar jet, the nozzle was 2mm long. Due to the low volumetric flow rate of coolant, it was measured at inlet and outlet from the cooling chamber with a graduated flask.

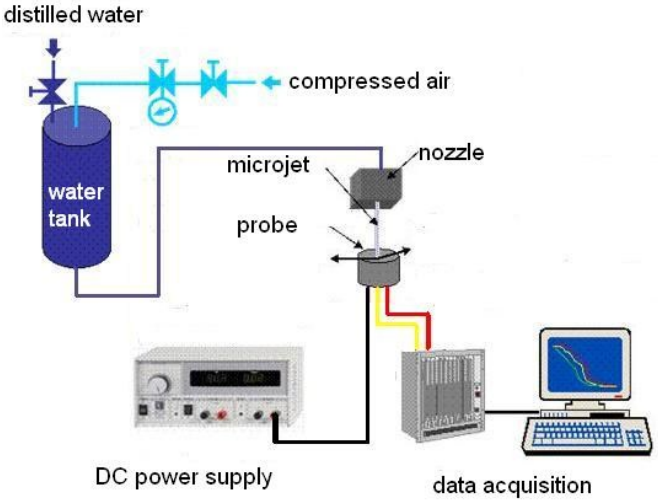

Fig.1 The schematic diagram of test section

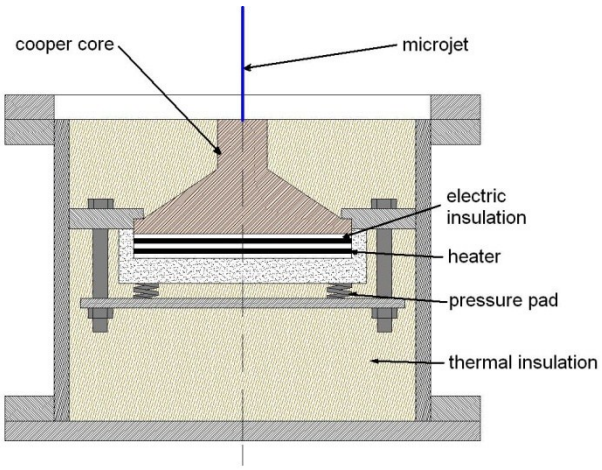

Fig.2 The cross-section of the probe

The cooled surface was the copper truncated cone with top diameter 10mm and 20mm height. Water impingement surface was silver-plated, in order to prevent high-temperature erosion. The radial distribution of surface temperature was determined with the aid of five T-type thermocouples, created from embedding 50μm thick constantan wire to the copper core. The heat was supplied by a canthal heater, electrically isolated with sapphire glass and mounted at the bottom of the core. The whole set was thermally insulated by glass wool and placed in the casing. The heater was powered by a DC power supply and the total power input was determined by measuring current intensity and voltage. During tests, the heater was capable of dissipating up to 240W.

Additional four K-type thermocouples are attached at the axis. These thermocouples measure axial temperature gradient at the core of a heating block and control temperature of the heater. All thermocouples are connected to the National Instruments data acquisition set. The signal was processed within specially developed LabVIEW application. Heater operating power values are precisely controlled and measured. The applied power losses through conduction into the insulation and radiation to the surroundings are accurately calculated and accounted for in all tests. Data are taken from a steady state measuring points in order to exclude heat capacity of the installation.

Nozzle construction allows modifying its dimensions. In the case of these studies, the nozzle with the dimensions of 50 x100 μm was used. Experiments were conducted for the spacing of 50mm between the nozzle exit and impinging surface. Experimental configuration allows for a free-surface unconfined jets flow. Because of a limited power supply, the low water mass flux was used in order to obtain a wide range of surface temperature. Uncertainties were calculated, for all measured and calculated parameters, according to the standard procedures described by NIST [20]. Overall, the uncertainty in the Nusselt number is around 2 - 7 %, with highest uncertainties obtained for ~10% of maximum heating power. Uncertainties in the other calculated variables are shown in Table 1.

Table 1. Measurement uncertainties.

Variable	*Uncertainty (%)*
(T_w-T_{in})	1.63%
G	1.5%
q	1.2%
Q	0.43%
h	1.97%
Re	2.59%
Nu	2.04%

Experimental procedure

Liquid distribution on the cooled surface is influenced by the presence of the neighboring microjets. Thus a number of adjoining and similar impingement cells are formed. The experimental setup is aimed at reproducing the conditions of CPU cooling. The effect of nozzle array geometry on the heat transfer characteristics was investigated by experimental runs, conducted with arrays consisting of 2, 3, 4 and 5 nozzles. Nozzle pitch was modified in the range from 1 to 5 mm. The geometry of nozzle array is presented in fig. 3. As mentioned, nozzle to surface distance was set at a constant height. Over 600 experimental data points under steady state conditions were obtained.

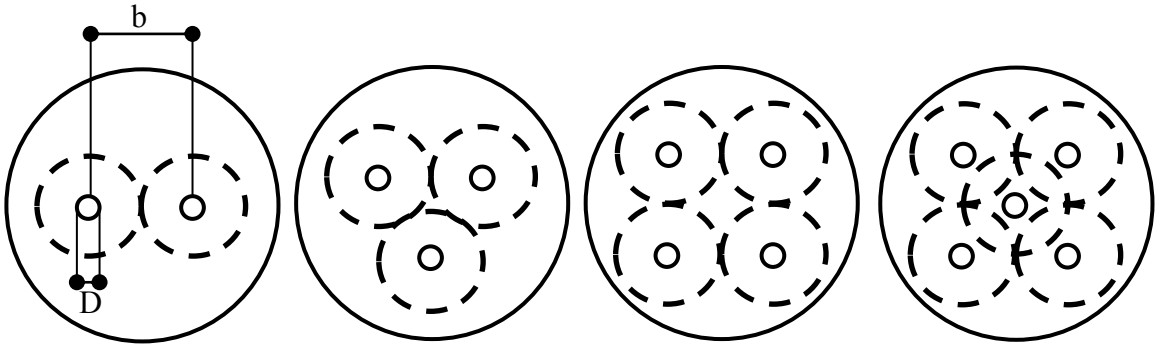

Fig.3 Representations of investigated microjet arrays

After setting up desired array geometry, supply pressure was set and power was supplied to the heater. Electrical power was fed in steps with increasing voltage. Average heat fluxes on the cooled surface were in the range of 40 to 1000 kW/m^2. The apparatus was considered to be in steady state operation when current test section temperatures were equal to averaged operating temperatures from last 2 min. Once the condition was verified, operating conditions were recorded and then new power parameters were set. After power adjustments, new operating conditions were observed after about 40-60 min. No testing was done with decreasing heat fluxes. Steady state temperatures in heater region measured on the copper core bottom surface were often as high as 200°C during tests. All materials of the test section (sealants and gaskets) were rated for continuous operation at temperatures up to 260°C. Water

supply system used in experiments constantly cooled down test section in the case of unintended power shortage.

Filtered and distilled water was used as a coolant. Long duration testing showed up a fouling build up on test surface. Additional tests for same geometrical and flow configurations were performed. No measurable shift on arrays heat transfer rates was noticed along these tests. Because of fouling, test routine included impingement surface cleaning, performed chemically every day by a weak acid solution. The test surface was cleaned from the oxide, the test surface was first immersed in a weak nitric acid solution (2% HNO3) for 5 min, and then thoroughly rinsed with de-ionized water. Variations of atmospheric pressure and temperature were monitored throughout the experiments, the boiling temperature of the working fluid remained near 100°C.

Data reduction

Based on the one-dimensional Fourier's law of conduction, heat flux q, through the impinged surface, can be calculated from the axial temperature variation, given by Eq. (1):

$$q = \frac{-k_b}{\delta x} \cdot \Delta T \tag{1}$$

where k_b is the thermal conductivity of the heating block and ΔT is the temperature difference from the heater to the test surface.

$$\Delta T = T_w - T_h \tag{2}$$

The test surface wall temperature T_w is area averaged temperature given by surface thermocouple readout, as given by Eq. (2).

$$T_w = \frac{\sum (T_i \cdot S_i)}{\sum S_i} \tag{3}$$

The heater was connected to a laboratory grade DC power supply. Thus the input electric power to the heater can be calculated by multiplying the measured electric current (I) and voltage (U). Assuming 100% heater efficiency, it is calculated as:

$$Q_{el} = I \times U \tag{4}$$

The test data in this study shows that Q_{el} and Q_c agree within 10%. This difference can be attributed to heat loss in heater casing. In order to calculate heat loss rate and diminish measurements error, heat loss data were taken for convective cooling of the probe, this resulted in a heat loss curve in function of heater temperature ($Q_{lo}=f(T_h)$). Heat transfer rate was calculated by substracting Q_{lo} from electrical power delivered to the test probe. Accordingly, the heat flux q on the cooled surface was calculated by dividing obtained result by cooled surface area.

$$q = \frac{Q_{el} - Q_{lo}}{A_c} \tag{5}$$

The average wall temperature (T_w) of the test surface was calculated accounting for the axial temperature variation, according to Eq. (3). The temperature difference was defined as the difference between the wall temperature (T_w) and the fluid inlet temperature (T_{in}). The average of these two readings was compared with saturation temperature corresponding to the measured system pressure. The heat transfer coefficient (h) is calculated by Eq. (6).

$$h = \frac{q}{T_w - T_{in}} \tag{6}$$

In Eq. (6), the heat flux (q) was calculated from the averaged heat flux on the cooled surface of the heating block. Hence, the heat transfer coefficient (h) is the area averaged heat transfer coefficient on the test surface. During the tests, the fluid inlet temperature (T_{in}) was set to 20°C, 80 K below the saturation temperature. The present jet cooling data were reduced to non-dimensional terms. The Nusselt number (Nu) is based on jet equivalent diameter and is defined by Eq. (7).

$$Nu = \frac{h \cdot D}{k_l} \tag{7}$$

Accordingly, the Reynolds number (Re) is defined. (8).

$$Re = \frac{G \cdot D}{\mu_l} \tag{8}$$

Fluid transport properties used to correlate various properties were evaluated for jet inlet temperature.

$$Pr = \frac{\mu_l \cdot c_{pl}}{k_l} \tag{9}$$

A superimposing technique is used to correlate heat transfer data for investigated jet patterns. In order to estimate jet spacing influence on heat transfer, data from authors previous experiments were taken [21]. Average Nusselt numbers for single microjet were correlated with eq. 10:

$$\overline{Nu_{jet}} = 0.9871 \cdot Re^{0.8843} \cdot Pr^{1.776} \cdot \left(\frac{D}{d}\right)^{1.897} \tag{10}$$

The interaction between multiple microjets in 3D space is very complicated. In this analysis, only configurations of microjets previously described in fig. 2 were considered in calculations.

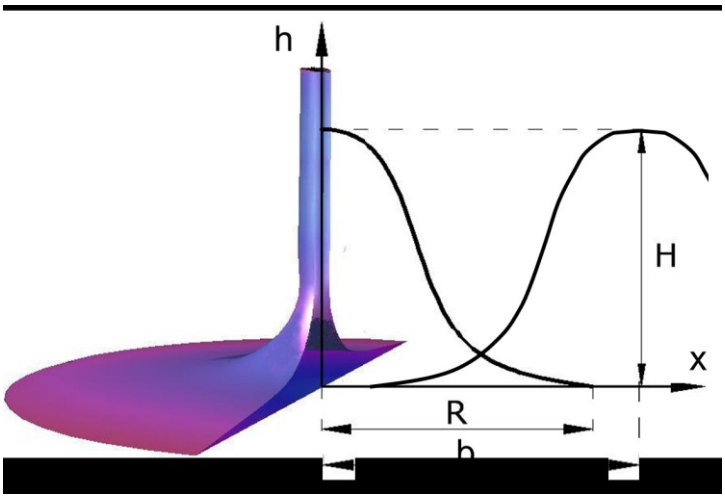

Fig.4 Scheme of impinging microjet heat transfer coefficient distribution

With equal nozzle to nozzle spacing in the jet array, superimposition of heat transfer coefficient on the cooled region can be simplified to a situation presented on fig.4. Therefore resulting HTC can be written as a function (11).

$$Nu = \phi\left(Nu_1 + Nu_2\right) = \phi\left[2\mathrm{H} - \frac{\mathrm{H}}{R}\left(2\mathrm{x} - b\right)\right] \tag{11}$$

Where φ is cooling contribution factor between adjacent microjets, and x is the radial distance from the stagnation point. If an array is made by identical nozzles distribution of Nusselt number Nu_1 and Nu_2 are also identical. Thus optimal jet to jet spacing, defined as the maximal Nusselt number would be obtained if jet to jet spacing was equal to jet's cooling radius (b=R).

In this paper, it is assumed that superposition of single microjet Nusselt number distributions depends on jets cooling radius R, and is constant for given experimental conditions. It can be rearranged as presented in eq. (12).

$$Nu = \phi\left(Nu_1 + Nu_2\right) = \phi(R) \tag{12}$$

Then average heat transfer coefficient on the cooled surface will also be dependent on parameter R. In order to present data in the non-dimensional form, it is divided by jets diameter.

$$\frac{Nu}{Nu_{jet}} = a \cdot \left(\frac{R}{D}\right)^b \tag{13}$$

The heat transfer will take place only if there is a temperature gradient between the fluid and cooled surface, thus the radius on which the liquid film is capable of heat transfer can be determined from the energy balance on the element of the cooled plate, as described in fig 5.

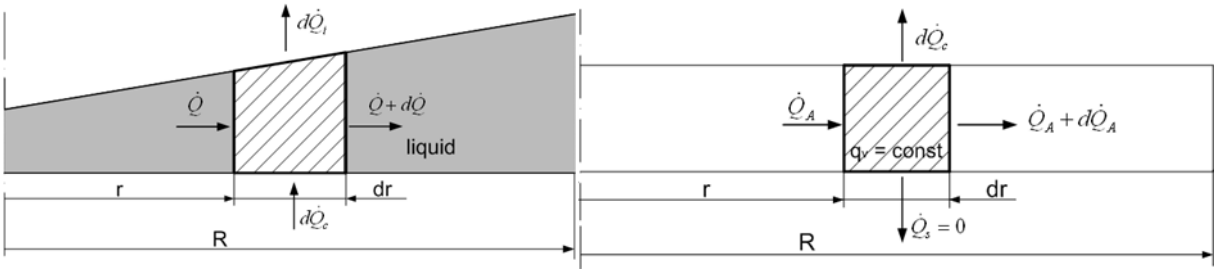

Fig.5 Energy balance at cooling fluid (left) and cooled plate(right)

From which energy equation reads as:

$$\dot{m} \cdot c_p \cdot \Delta t = q \cdot \pi \cdot R^2 \tag{14}$$

From eq.(14) jet cooling radius is:

$$R = \sqrt{\frac{\dot{m} \cdot c_p \cdot \Delta t}{\pi \cdot \dot{q}}} \tag{15}$$

Searching the above expression, we have recourse to the experimentally obtained correlation for a single microjet, comparing it to the heat transfer coefficients obtained experimentally for microjet arrays.

$$\frac{Nu_{exp}}{Nu_{jet}} = c_1 \cdot \left(\frac{R}{D}\right)^{c_2} \tag{16}$$

Equation (16) represents the partial solution, for which we obtain the most uniform distribution of heat transfer coefficient on the cooled surface.

Of course, this approximation takes into account only two jets to take into account the spatial distribution of the nozzles, authors introduce an additional correction factor takes into account the ratio of the nozzles used in the array to a number of optimal nozzles:

$$\frac{Nu_{exp}}{Nu_{jet}} = c_1 \cdot \left(\frac{n}{n_{opt}}\right)^{c_3} \tag{17}$$

The optimal number of jets used in eq. 17 can be determined for a given surface, as the ratio of the cooled surface area (S) to the area of a single jet efficient cooling surface:

$$\frac{S}{\pi \cdot R^2} = n_{opt} \tag{18}$$

As a result, a final correlation for an area averaged heat transfer coefficient, is a function of single microjet heat transfer:

$$Nu_{exp} = c_1 \cdot Nu_{jet} \cdot \left(\frac{R}{D}\right)^{c_2} \cdot \left(\frac{n}{n_{opt}}\right)^{c_3} \tag{19}$$

Correlation coefficients c_1, c_2, and c_3 are to be obtained experimentally.

Experimental validation

Heat transfer experiments were preceded by the calibration of the microjets volumetric flow rate. The flow from the nozzle is controlled by maintaining a constant pressure in the supply tank. For selected nozzle geometries, the nozzle flow characteristics were determined according to the overpressure generated in the nozzle feed. With array of jets only water mass flow rate changes $\dot{m}$, the Reynolds number and mass flux are same for all of the configurations. Fig. 6 presents obtained mass flux and Reynolds number values obtained with constant supply pressure. Experiments were performed for two values of supplying pressure 100 and 200kPa, corresponding to *Re*=1350 and 2050.

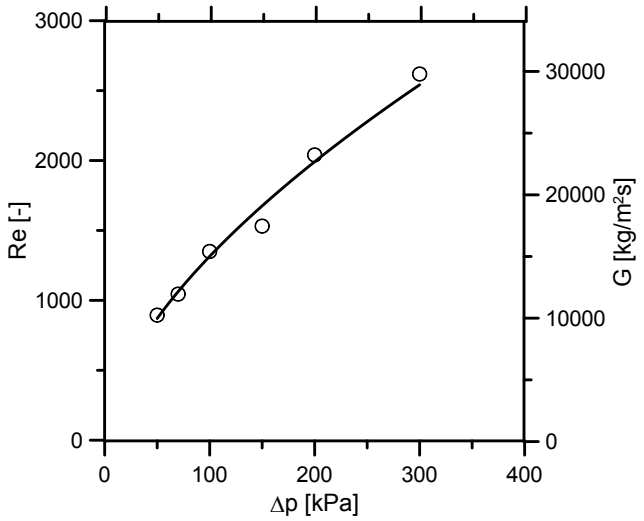

Fig.6. Pressure drop characteristics of the tested nozzle

Fig. 7 shows the experimental results of heat transfer rate for impinging water jet using the nozzle equivalent diameter of *D*=80μm. Heat transfer data are plotted in the form of boiling curves for different fluid flow rates. As reported in literature higher jet velocities allow obtaining higher heat transfer rates, resulting in lower surface temperature for supplying heat flux. Also, as depicted in Fig. 8 for the set of two microjets similar shifts can be observed with the varying jet to jet spacing. This shift is not linear, therefore it is expected that optimal nozzle spacing can be found.

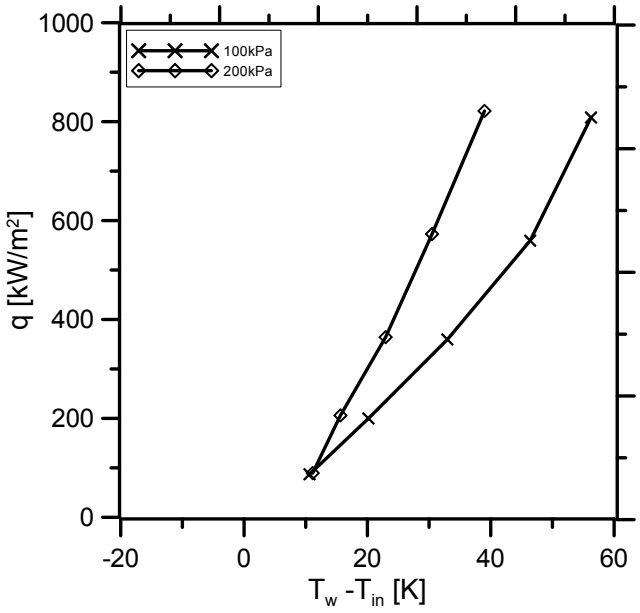

Fig. 7. Heat flux density in function of wall temperature for 5 nozzle array

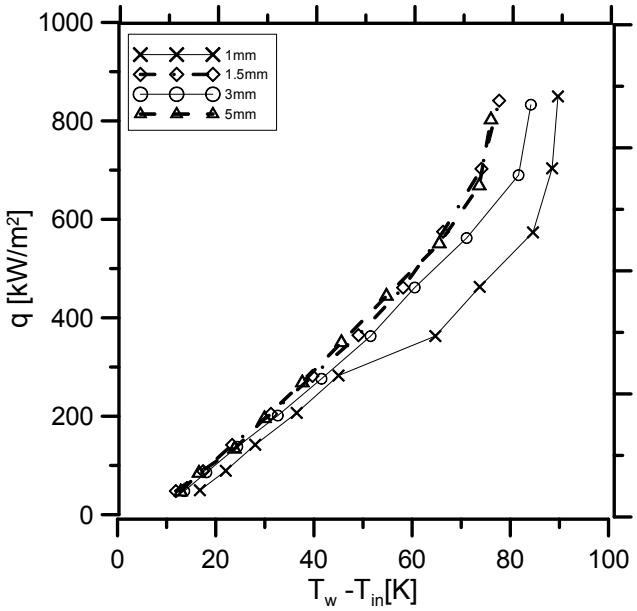

Fig. 8. Wall temperature in function of heat flux, for varying jet spacing 2x0.1mm

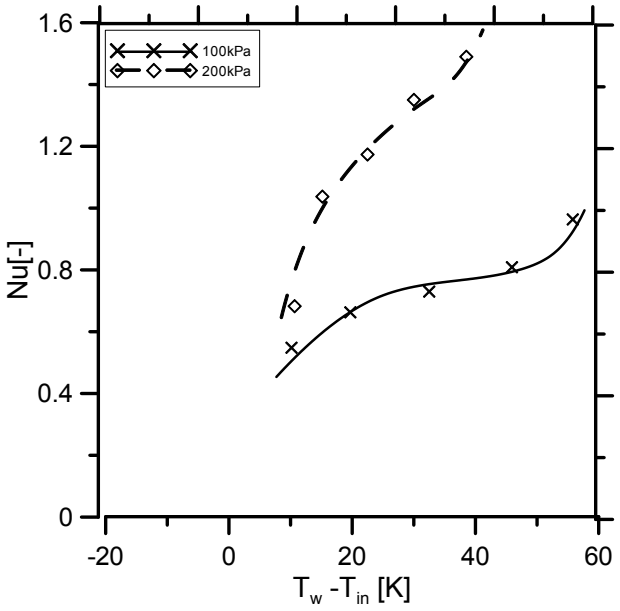

Fig. 9. Area averaged Nusselt number for 5 nozzle array

In order to verify the theoretical model, data points from experimental series were collected. in which the surface temperature does not exceed the saturation temperature of the coolant - water. Then, based on physical database fluids REFPROP [22] is specified heat transfer coefficient in the form of the dimensionless Nusselt number. Resulting area averaged Nusselt numbers for the array of five microjets is presented on fig. 9. As can be seen for the constant fluid flow rate the HTC is increasing with increased surface temperature. For constant fluid flow rate (constant supply pressure), only increased heat flux affects the obtained heat transfer coefficient. According to eq. (15) the effective cooling radius of the microjet is changing, thus the interaction between the microjets is affected.

For better compatibility of a mathematical model with the experiment, previously obtained correlation [21] describing the heat transfer coefficient for a single water microjet was used:

$$Nu_{jet} = 0.9871 \cdot \mathrm{Re}^{0.8843} \cdot \mathrm{Pr}^{1.776} \cdot \left(\frac{D}{d}\right)^{1.897} \tag{20}$$

Presented correlation was further used to obtain experimental factors of the jet to jet contribution factor as a function of array geometrical dimensions. Figure 1 depicts data best fit to proposed correlation by adjusting c_1, c_2 and c_3 parameters from eq. (19). Final representation of experimental correlation is given in eq. (21).

$$Nu_{exp} = 0.36 \cdot Nu_{jet} \cdot \left(\frac{R}{D}\right)^{-0.487} \cdot \left(\frac{n}{n_{opt}}\right)^{-0.38} \quad \textbf{(21)}$$

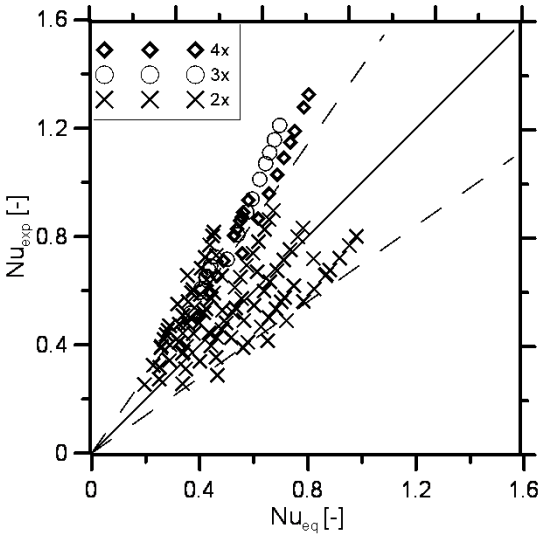

Fig. 10. Experimentally obtained, area averaged Nusselt numbers vs. predictions by eq. (21)

Obtained HTC in the dimensionless form of the Nusselt number was also successfully used to predict average surface temperature. Predicted values were used to calculate the energy balance on the surface Eq.(14). As a simplification authors assumed uniform liquid film distribution from impingement point, just as in single microjet case. Temperature predictions, given simplification by Eq.(21) are presented in fig. 11 and 12. It needs to be noted that larger scatter of data with two microjets is attributed to the fact that it comprises series with the varying jet to jet distance. In the case of two microjets, a higher distance between microjets causes larger flow nonuniformity over the cooled surface.

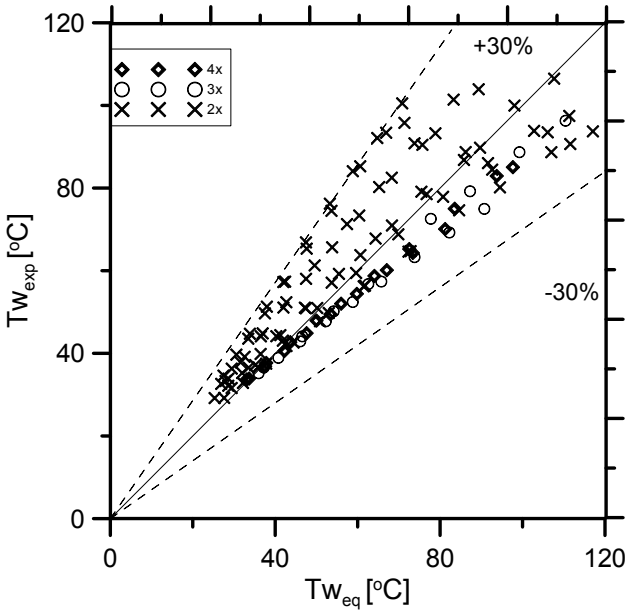

Fig. 11. Temperature predictions with Eq.(21) vs. experimental data

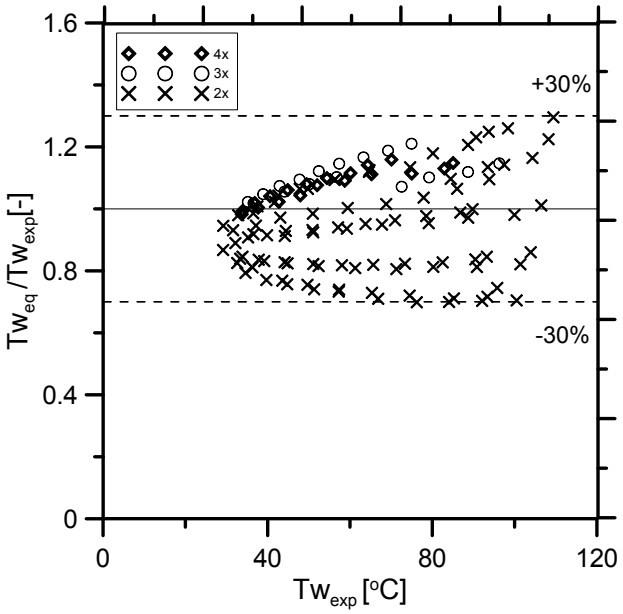

Fig. 12. Temperature predictions with Eq.(21) vs. experimental data

Due to the high thermal capacity of water, microjet cooling is capable of removing large heat quantities, with low volumetric flow rate. The economy of a thermal management system is increased if its capacity is fully used. Fig. 13 shows the experimental effectiveness of heat removal by the array and single microjet impingement. The effectiveness of heat exchange performance was described as theoretical pumping power P_p, divided by transferred heat $\dot{Q}_{ch}$.

Pumping power was expressed as total pressure drop measured in cooling system times the volumetric flow rate of water, eq. (22).

$$P_p = \dot{V}\Delta P \tag{22}$$

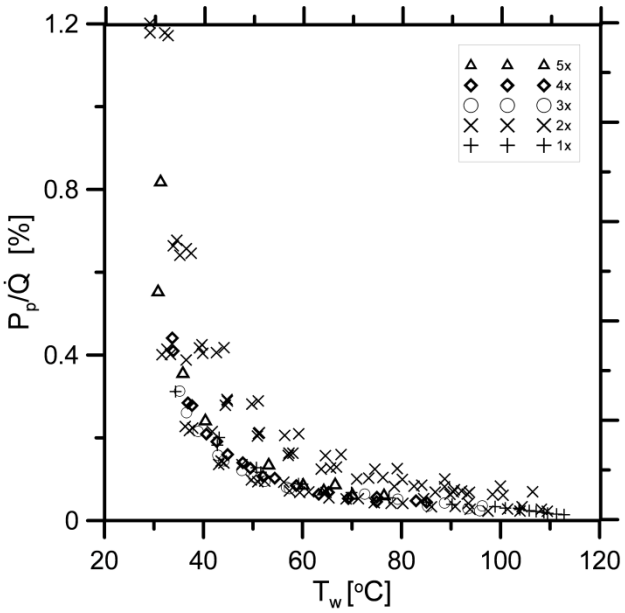

Fig. 13. Heat flux density in function of wall temperature for 5 nozzle array

As can be seen, an array of microjets can remove heat more efficiently. Unfortunately, in some cases set of two microjets (x) gives worse cooling effect than single microjet. Therefore in authors opinion, it is crucial to optimize jet array dimensions according to proposed correlation.

Conclusions

The experimental research of single phase heat transfer due to impingement of microjet array of water was studied on a specially designed rig. Systematic data on wall temperature and dissipated heat has been collected, which enabled development of empirical correlation for the Nusselt number. The model shows very good consistency with experimental data within the error margin of 30%. Qualitatively, the model returns good results which allow the discussion of the influence of various parameters on temperature field and optimize the thermal load of cooled surface. Such tool would be very helpful in the planning of experiments with other

cooling fluids. The difference in radial temperature distribution authors attributes to assumptions of uniform heat flux on the cooled surface and uniform flow field.

A simple form of distribution of wall temperature and cooling fluid temperature obtained in the analytical model is of a great value when the sensitivity tests are to be carried out. That will enable, for example, the optimization of geometrical parameters for described thermal management systems. The model is quite general and its further modifications are possible when some of the assumptions are relaxed. The performance of presented model depends very strongly on the distribution of heat transfer coefficient. More experiments on the influence of microjet arrays are needed which will confirm the heat transfer coefficient correlation presented in the paper.

Nomenclature

A	m^2	surface area
b	m	jet to jet distance
c_p	J/kg K	specific heat
c_1,c_2,c_3		empirical constants
d	m	Cooled surface diameter
D	m	jet diameter
ΔP	kPa	pressure drop in the nozzle
g	m/s^2	gravitational acceleration
G	kg/m^2s	jet mass flux
h	W/m^2K	heat transfer coefficient
H	W/m^2K	peak heat transfer coefficient
I	A	current

k	W/m^2K	Thermal conductivity
$\dot{m}$	kg/s	mass flow rate
n		Number of jets
Nu		Nusselt number
P	W	Power
Pr		Prandtl number
$\dot{Q}$	W	Heat flux
Re		Reynolds number
ρ	kg/m^3	density
S	m^2	Surface area
q	W/m^2	Heat flux density
T	K	temperature
U	V	voltage
$\dot{V}$	m^3/s	volumetric flow rate
x	m	distance

Subscripts

air	air
b	copper block
c	cooling
el	electric
exp	experimental

in	inlet
jet	jet parameter
l	liquid
h	heater parameter
opt	optimal number
p	pump
w	wall parameter

References

[1] T. Muszynski, S.M. Koziel, Parametric study of fluid flow and heat transfer over louvered fins of air heat pump evaporator, Arch. Thermodyn. 37 (2016) 45–62. doi:10.1515/aoter-2016-0019.

[2] P. Smakulski, S. Pietrowicz, A review of the capabilities of high heat flux removal by porous materials, microchannels and spray cooling techniques, Appl. Therm. Eng. 104 (2016) 636–646. doi:10.1016/j.applthermaleng.2016.05.096.

[3] Z. Meng, Z. Meng, W. Lu, Z. Zhu, Y. Sun, Research on heat exchange and control method of the evaporative condenser in the equipment of flax fiber modification, Appl. Therm. Eng. 100 (2016) 595–601. doi:10.1016/j.applthermaleng.2016.02.011.

[4] R.S. Andhare, A. Shooshtari, S. V. Dessiatoun, M.M. Ohadi, Heat transfer and pressure drop characteristics of a flat plate manifold microchannel heat exchanger in counter flow configuration, Appl. Therm. Eng. 96 (2016) 187–189. doi:10.1016/j.applthermaleng.2015.10.133.

[5] G.J. Michna, E.A. Browne, Y. Peles, M.K. Jensen, The effect of area ratio on microjet array heat transfer, Int. J. Heat Mass Transf. 54 (2011) 1782–1790. doi:10.1016/j.ijheatmasstransfer.2010.12.038.

[6] T. Muszynski, D. Mikielewicz, Comparison of heat transfer characteristics in surface cooling with boiling microjets of water, ethanol and HFE7100, Appl. Therm. Eng. 93 (2016) 1403–1409. doi:10.1016/j.applthermaleng.2015.08.107.

[7] T. Muszynski, R. Andrzejczyk, Heat transfer characteristics of hybrid microjet – Microchannel cooling module, Appl. Therm. Eng. 93 (2016) 1360–1366. doi:10.1016/j.applthermaleng.2015.08.085.

[8] A. Husain, M. Ariz, N.Z.H. Al-Rawahi, M.Z. Ansari, Thermal performance analysis of a hybrid micro-channel, -pillar and -jet impingement heat sink, Appl. Therm. Eng. 102 (2016) 989–1000. doi:10.1016/j.applthermaleng.2016.03.048.

[9] C.Y. Li, S. V. Garimella, Prandtl-number effects and generalized correlations for confined and submerged jet impingement, Int. J. Heat Mass Transf. 44 (2001) 3471–3480. doi:10.1016/S0017-9310(01)00003-5.

[10] L. Qiu, S. Dubey, F.H. Choo, F. Duan, The jet impingement boiling heat transfer with ad hoc wall thermal boundary conditions, Appl. Therm. Eng. 108 (2016) 456–465. doi:10.1016/j.applthermaleng.2016.07.134.

[11] R. Andrzejczyk, T. Muszynski, C. Alberto Dorao, Experimental investigations on adiabatic frictional pressure drops of R134a during flow in 5mm diameter channel, Exp. Therm. Fluid Sci. 83 (2017) 78–87. doi:10.1016/j.expthermflusci.2016.12.016.

[12] L. Qiu, S. Dubey, F.H. Choo, F. Duan, Recent developments of jet impingement nucleate boiling, Int. J. Heat Mass Transf. 89 (2015) 42–58. doi:10.1016/j.ijheatmasstransfer.2015.05.025.

[13] E.A. Browne, G.J. Michna, M.K. Jensen, Y. Peles, Microjet array single-phase and flow boiling heat transfer with R134a, Int. J. Heat Mass Transf. 53 (2010) 5027–5034. doi:10.1016/j.ijheatmasstransfer.2010.07.062.

[14] B.P. Whelan, A.J. Robinson, Nozzle geometry effects in liquid jet array impingement, Appl. Therm. Eng. 29 (2009) 2211–2221. doi:10.1016/j.applthermaleng.2008.11.003.

[15] D.R.H. Gillespie, Z. Wang, P.T. Ireland, S.T. Kohler, Full surface local heat transfer coefficient measurements in a model of an integrally cast impingement cooling geometry, J. Turbomach. 120 (1998) 92–99.

[16] T. Muszynski, R. Andrzejczyk, Applicability of arrays of microjet heat transfer correlations to design compact heat exchangers, Appl. Therm. Eng. 100 (2016) 105–113. doi:10.1016/j.applthermaleng.2016.01.120.

[17] T. Muszynski, Design And Experimental Investigations Of A Cylindrical Microjet Heat Exchanger For Waste Heat Recovery Systems, Appl. Therm. Eng. (2017). doi:10.1016/j.applthermaleng.2017.01.021.

[18] N. Tran, Y.-J. Chang, J.-T. Teng, R. Greif, Enhancement heat transfer rate per unit volume of microchannel heat exchanger by using a novel multi-nozzle structure on cool side, Int. J. Heat Mass Transf. 109 (2017) 1031–1043. doi:10.1016/j.ijheatmasstransfer.2017.02.058.

[19] N. Karwa, C. Stanley, H. Intwala, G. Rosengarten, Development of a low thermal resistance water jet cooled heat sink for thermoelectric refrigerators, Appl. Therm. Eng. 111 (2017) 1596–1602. doi:10.1016/j.applthermaleng.2016.06.118.

[20] B.N. Taylor, C.E. Kuyatt, Guidelines for Evaluating and Expressing the Uncertainty of NIST Measurement Results, (n.d.).

[21] D. Mikielewicz, T. Muszynski, Comparison of Heat Transfer Characteristics in Surface Cooling With Boiling Microjets of Water , Ethanol and, in: Janusz T. Cieśliński (Ed.), XXI Int. Symp. Reserch-Education-Technology, Gdansk University of Technology, 2013: pp. 1–9.

[22] E.W. Lemmon, M.L. Huber, M.O. McLinden, NIST Standard Reference Database 23: Reference Fluid Thermodynamic and Transport Properties (REFPROP), Version 9.0, Phys. Chem. Prop. …. (2010).